Experimental Demo of Range Disambiguation via Slow-time Coding & Reiterative Super-Resolution

Jennifer E. Quirk, Patrick M. McCormick, Jonathan W. Owen, Shannon D. Blunt
Radar Systems Lab (RSL), University of Kansas, Lawrence, KS

***Abstract*—Slow-time coding (STC) has previously been examined for multiple-input multiple-output (MIMO) radar and disambiguation of multiple range ambiguities. However, using STC with non-adaptive Doppler processing often results in high Doppler "cross-ambiguity" sidelobes that can hinder range disambiguation despite the degree of separability imparted by STC. To enhance this separability, a "multi-range" (MR) modification to the reiterative super-resolution (RISR) approach is examined that accounts for the distinct range interval structure from STC and is denoted as MR-RISR. The efficacy of this implementation is examined using open-air measurements. Further, incorporation of clutter cancellation via the previously developed background supplementary cancellation (BaSC) arrangement is shown to yield further improvement by reducing the necessary dynamic range for which Doppler estimation is needed.**

Keywords—range-folded scattering, range ambiguity, slow-time coding, waveform diversity, adaptive processing

I. Introduction

Much of the existing research on slow-time coding (STC) relates to MIMO waveform design [1-8], subsuming the particular case of Doppler-division multiple access (DDMA) and variations thereof [6-8]. In [9], analysis of the signal model that incorporates STC and/or staggered pulse repetition interval (PRI) leads to the idea of a Doppler manifold, conceptually analogous to an antenna array manifold [10,11]. The Doppler manifold invokes a modification to the standard uniform PRI Doppler steering vectors. When uniform PRIs are combined with STC, the Doppler manifold results in a modified Doppler response while retaining the unambiguous Doppler extent on $f_{\rm D} \in [-\text{PRF}/2, +\text{PRF}/2]$. Consequently, standard Doppler processing across pulses (i.e. a discrete Fourier transform (DFT) with a single Doppler manifold) now requires modest compensation for adequate scattering estimation.

Separately, "beyond linear processing" [12] methods are under exploration to enhance Doppler estimation for both uniform and staggered PRI transmissions. For instance, [13] experimentally demonstrated that nonlinear processing via the reiterative super-resolution (RISR) algorithm improves pulse-Doppler estimation significantly in comparison to standard Doppler processing. The RISR algorithm is a specific instantiation of the reiterative minimum mean squared error (RMMSE) framework. Due to implicit similarities between slow-time Doppler [13], fast-time space [14], and fast-time frequency [15] models, variations of the RISR algorithm have been implemented in each domain. The RMMSE framework has also been employed in the range [16] and joint range/Doppler dimensions [17], with open-air demonstration shown in [18]. With proper clutter estimation, RISR can be paired with clutter suppression via background supplementary cancellation (BaSC) [19], which is a direct extension of maximum SINR filtering [20].

Code diversity implies that STC lends itself to receive processing in a range-folded or multiple-time-around (MTA) scenario [21-24]. That is, each range interval exhibits a modified Doppler manifold, thus allowing for range disambiguation due to the attendant quasi-orthogonality. In practice, STC enables disambiguation of MTA scattering relative to the available degrees-of-freedom. For instance, minimum variance distortionless response (MVDR) filtering has been examined [25] to minimize Doppler sidelobes when using STC and PRI staggering for range disambiguation.

Here, random uniformly distributed STC is encoded onto linear frequency modulation (LFM) waveforms and then transmitted with a uniform PRI in an open-air setting. The existing MTA scattering is separated into the proper range intervals (verified by subsequent unambiguous transmission). Doppler processing with STC modification demonstrates an adequate degree of target separability for overlapping range returns. For improved performance, the RISR formulation is then modified to jointly estimate and separate multiple range ambiguities for STC transmit sequences. The multi-range RISR (MR-RISR) approach demonstrates enhanced scatterer estimation within the designated range intervals, limited only by system fidelity and model mismatch effects. Employing MR-RISR in the BaSC [19] context yields further enhancement via multi-range clutter cancellation.

II. Slow-Time Coding (STC) Signal Model

Consider a pulse-Doppler radar transmitting M pulses at a uniform PRI denoted as $T_{\rm PRI}$ within a coherent processing interval (CPI) $T_{\rm CPI}$, where each pulse is modulated by the same waveform $s(t)$ having pulse duration τ and 3-dB bandwidth B. To apply a STC sequence across the CPI, the $m^{\rm th}$ pulse is modulated by an arbitrary phase value $-\pi \leq \theta_m \leq \pi$. The transmitted pulse therefore takes the form

$$s_m(t) = s(t)e^{j\theta_m} \ \text{ for } \ t \in (0, \tau)\,. \tag{1}$$

For now, assume that the PRI is long enough that multiple-time-around (MTA) clutter can be ignored. The received slow-time coded scattering that includes radial movers can thus be expressed for the $m^{\rm th}$ pulse as

This work was supported in part by the Office of Naval Research under Contract #N00014-23-C-1053 and by a subcontract with Systems & Technology Research for the Defense Advanced Research Projects Agency under Prime Contract #FA2385-23-C-0004. DISTRIBUTION STATEMENT A. Approved for Public Release.

$$y(m,t) = \left[\sum_{f_D}\left[s(t;f_D) * x(t;f_D)\right]e^{j(2\pi f_D(m-1)T_{PRI}+\theta_m)} + n(m,t)\right] \times \mathrm{rect}(\tau, T_{PRI}) \quad (2)$$

for time interval $t \in [0, T_{PRI}]$. Here $x(t;f_D)$ represents the illuminated range profile of arbitrary scattering having Doppler frequency $f_D = 2v/\lambda$ Hz (for radial velocity v and wavelength λ). Then

$$s(t;f_D) = s(t)e^{j2\pi f_D t} \text{ for } t \in (0,\tau) \quad (3)$$

is the fast-time Doppler-shifted version of the transmitted waveform (ignoring relativistic effects), the operation $*$ denotes convolution, and $n(m,t)$ is zero-mean white Gaussian noise with noise power $\sigma_n{}^2$. With normalized Doppler defined as

$$f_{nD} = f_D T_{PRI}\,, \quad (4)$$

it is convenient to rewrite (2) in terms of normalized quantities as

$$y(m,t) = \left[\sum_{f_D}\left[s(t;f_D) * x(t;f_D)\right]e^{j(2\pi(m-1)f_{nD}+\theta_m)} + n(m,t)\right] \times \mathrm{rect}(\tau, T_{PRI}) \,, \quad (5)$$

where the STC component is now part of the exponent term.

When MTA effects are present, the model from (5) is superimposed with additional scattering from prior pulse transmissions. The number of observable range intervals G indicates the number of adjacent PRI durations, which must be disambiguated during radar processing. The user-defined radar listening interval GT_{PRI} then determines the maximum observable range. For G observable range intervals, $G-1$ fill pulses [9] are needed so that scattering from all G range intervals superimpose in each ensuing PRI for all M pulses. Denoting the G^{th} pulse as the "beginning" of the CPI (for processing), then $m = 1, 2, \ldots, G-1$ indexed pulses are the fill pulses and the $m = G, G+1, \ldots, G+M-1$ indexed pulses comprise the CPI with M PRIs exhibiting G superimposed range intervals, as illustrated in Fig. 1.

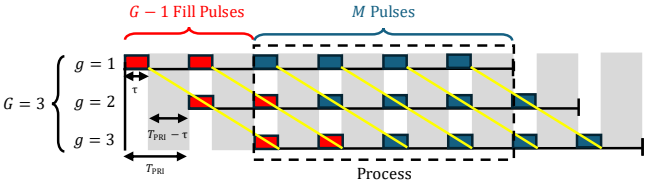

Fig. 1: Illustration of fill pulses and overlapped range intervals. Each additional delay of T_{PRI} shifts the observed pulses through the specified range intervals. For this example ($G = 3$), time segments where all G range intervals overlap are processed with STC separation via quasi-orthogonal Doppler manifolds.

With superimposed MTA from prior range intervals, the receive signal in (5) of the current listening interval for pulse indices $m = G, G+1, \ldots, G+M-1$ can be generalized to

$$y(m,t) = \left(\sum_{f_D}\left[s(t;f_D) * x(t;f_D)\right]e^{j(2\pi(m-1)f_{nD}+\theta_m)} + n(m,t) + \sum_{g=2}^{G}\sum_{f_D}\left[s(t;f_D) * x(t+(m-g+1)T_{PRI};f_D)\right]e^{j(2\pi(m-g)f_{nD}+\theta_{m-g+1})}\right) \times \mathrm{rect}(\tau, T_{PRI}) \quad (6)$$

for time interval $t \in [0, T_{PRI}]$. The first line of (6) corresponds to the first range interval ($g = 1$) while the summation on the second line captures the remaining $(G-1)$ MTA intervals.

Discretizing (6) *in the fast-time dimension* then yields a discrete linear representation for the m^{th} PRI as

$$\begin{aligned}\mathbf{y}(m) &= \left(\sum_{f_D}\mathbf{S}(f_D)\mathbf{x}_1(f_D)e^{j(2\pi(m-1)f_{nD}+\theta_m)} + \mathbf{n}(m) + \sum_{g=2}^{G}\sum_{f_D}\mathbf{S}(f_D)\mathbf{x}_g(f_D)e^{j(2\pi(m-g)f_{nD}+\theta_{m-g+1})}\right) \\ &= \sum_{g=1}^{G}\sum_{f_D}\mathbf{S}(f_D)\mathbf{x}_g(f_D)e^{j(2\pi(m-g)f_{nD}+\theta_{m-g+1})} \end{aligned} \quad (7)$$

where $\mathbf{S}(f_D)$ is a convolution matrix of the sampled fast-time Doppler-shifted signal $s(t;f_D)$, vector $\mathbf{x}_g(f_D)$ is the arbitrary range scattering for Doppler shift f_D from the g^{th} observable range interval, and $\mathbf{n}(m)$ is the noise collected during the m^{th} PRI. For model simplification, we shall approximate fast-time Doppler effects as negligible via the stop-and-hop assumption such that $\mathbf{S}(f_D) = \mathbf{S}(0) \to \mathbf{S}$. Pulse compression with a zero-Doppler shifted waveform replica for each range interval is then

$$\begin{aligned}\bar{\mathbf{z}}(m) &= \mathbf{S}^H\left(\sum_{g=1}^{G}\sum_{f_D}\mathbf{S}\mathbf{x}_g(f_D)e^{j(2\pi(m-g)f_{nD}+\theta_{m-g+1})} + \mathbf{n}(m)\right) \\ &= \sum_{g=1}^{G}\sum_{f_D}\bar{\mathbf{x}}_g(f_D)e^{j(2\pi(m-g)f_{nD}+\theta_{m-g+1})} + \mathbf{S}^H\mathbf{n}(m)\,, \end{aligned} \quad (8)$$

where $\bar{\mathbf{x}}_g(f_D)$ is a version of $\mathbf{x}_g(f_D)$ shaped by pulse compression. Furthermore, since each of the $g = 1, 2, \ldots, G$ range intervals have a distinct STC structure, the Doppler steering vector of the g^{th} range interval can be defined (per [9]) according to the argument of the complex exponential from (8) as

$$\begin{aligned}\mathbf{v}_g(f_{nD}) &= \left[e^{j\theta_{G+1}} \quad e^{j[2\pi(1)f_{nD}+\theta_{G+2}]} \quad \ldots \quad e^{j[2\pi(M-1)f_{nD}+\theta_{G+M}]}\right]^T \\ &= \mathbf{v}(f_{nD}) \odot \mathbf{d}(\boldsymbol{\theta}_g), \end{aligned} \quad (9)$$

where $\odot$ is the Hadamard product, $G = G - g$ for notational convenience, $\mathbf{v}(f_{nD})$ has the standard Vandermonde form

$$\bar{\mathbf{v}}(f_{nD}) = [1 \quad e^{j2\pi(1)f_{nD}} \quad \ldots \quad e^{j2\pi(M-1)f_{nD}}]^T, \quad (10)$$

and $\mathbf{d}(\boldsymbol{\theta}_g)$ is a phase deviation vector that collects the STC sequence as

$$\mathbf{d}(\boldsymbol{\theta}_g) = [e^{j\theta_{G+1}} \quad e^{j\theta_{G+2}} \quad \ldots \quad e^{j\theta_{G+M}}]^T. \quad (11)$$

The implication of (11) is a unique Doppler manifold associated with each range interval g, therefore enabling separability between scattering from each range interval. By collecting versions of (9) for some discretization of Doppler (for vector $\mathbf{f}_{\text{nD}}$), the Doppler steering matrix for the g^{th} interval of dimension $M \times N$ can thus be expressed as

$$\begin{aligned}\mathbf{V}_g &= \exp\left\{ j2\pi \boldsymbol{\varepsilon}_{\text{acc}} \mathbf{f}_{\text{nD}}^T \right\} \odot [\mathbf{d}(\boldsymbol{\theta}_g)\mathbf{1}^T] \\ &= \overline{\mathbf{V}}_g \odot \mathbf{D}(\boldsymbol{\theta}_g),\end{aligned} \tag{12}$$

where $\boldsymbol{\varepsilon}_{\text{acc}} = [0 \quad 1 \quad \cdots \quad M-1]^T$.

III. Doppler Processing Techniques

We now consider the impact of STC on Doppler processing. A variant of the RISR method, which has previously been experimentally demonstrated for adaptive Doppler processing, is then posed to disambiguate range intervals.

A. Clutter Cancellation

Using (12), the pulse compressed signal model of (8) can also be discretized *in the slow-time dimension* for the ℓ^{th} range index snapshot to realize the $M \times 1$ vector

$$\overline{\mathbf{z}}(\ell) = \sum_{g=1}^{G} \mathbf{V}_g \overline{\mathbf{x}}_g(\ell) + \mathbf{n}(\ell), \tag{13}$$

where $\overline{\mathbf{x}}_g(\ell)$ of size $N \times 1$ contains the Doppler-dependent complex amplitudes we wish to estimate for range bin ℓ (after pulse compression), matrix $\mathbf{V}_g$ is from (12), and $\mathbf{n}$ is an $M \times 1$ vector of zero-mean white Gaussian noise with noise power ${\sigma_{\text{n}}}^2$.

For some specific range interval $\overline{g}$, standard Doppler processing (SDP) can be performed as

$$\begin{aligned}\mathbf{x}_{\text{MF},\overline{g}}(\ell) &= \mathbf{W}_{\text{MF},\overline{g}}^H \overline{\mathbf{z}}(\ell) \\ &= \mathbf{V}_{\overline{g}}^H \left(\sum_{g=1}^{G} \mathbf{V}_g \overline{\mathbf{x}}_g(\ell) \right) + \mathbf{V}_{\overline{g}}^H \mathbf{n}(\ell).\end{aligned} \tag{14}$$

Per (13), $\overline{\mathbf{z}}(\ell)$ contains scattering from all G range intervals. Attempting to perform Doppler processing using some $\mathbf{W} = \mathbf{V}_{\overline{g}}$ yields coherent matching to scattering received from the $\overline{g}^{\text{th}}$ range interval but is incoherent to the other $g \neq \overline{g}$ range intervals. This effect may be problematic when high-power clutter is present in multiple range intervals since the clutter responses from the $g \neq \overline{g}$ range intervals (which typically spread across all Doppler) may overwhelm the responses of interest from the $\overline{g}^{\text{th}}$ range interval.

Background supplementary cancellation (BaSC) is the nomenclature introduced in [19] whereby standard clutter cancellation is combined with adaptive Doppler estimation. We see that (13) can be decomposed as

$$\begin{aligned}\overline{\mathbf{z}}(\ell) &= \sum_{g=1}^{G} \mathbf{V}_g \overline{\mathbf{x}}_{\text{clut},g}(\ell) + \sum_{g=1}^{G} \mathbf{V}_g \overline{\mathbf{x}}_{\text{mov},g}(\ell) + \mathbf{n} \\ &= \overline{\mathbf{z}}_{\text{clut}}(\ell) + \overline{\mathbf{z}}_{\text{mov}}(\ell) + \mathbf{n},\end{aligned} \tag{15}$$

where $\overline{\mathbf{x}}_{\text{clut},g}(\ell)$ and $\overline{\mathbf{x}}_{\text{mov},g}(\ell)$ correspond to the clutter and movers, respectively, observed at the ℓ^{th} range bin in the g^{th} range interval, and

$$\mathbf{R}_{\text{clut}}(\ell) = \mathscr{E}\left[\overline{\mathbf{z}}_{\text{clut}}(\ell) \overline{\mathbf{z}}_{\text{clut}}^H(\ell) \right] \tag{16}$$

for $\mathscr{E}[\cdot]$ denoting expectation. Note that $\overline{\mathbf{z}}_{\text{clut}}(\ell)$ in (15) and (16) subsumes the clutter across all G range intervals. Then define the normalized cancellation matrix as

$$\begin{aligned}\mathbf{R}_{\text{canc}}(\ell) &= \frac{\mathbf{R}_{\text{clut}}(\ell) + \mathbf{R}_{\text{n}}}{{\sigma_{\text{n}}}^2} \\ &= \frac{\mathbf{R}_{\text{clut}}(\ell) + {\sigma_{\text{n}}}^2 \mathbf{I}}{{\sigma_{\text{n}}}^2},\end{aligned} \tag{17}$$

the inverse of which projects the non-clutter components of (13) onto the orthogonal complement of the clutter subspace while preserving full-rank noise. Specifically, the BaSC approach [19] applies

$$\begin{aligned}\mathbf{z}(\ell) &= \mathbf{R}_{\text{canc}}^{-1}(\ell)\, \overline{\mathbf{z}}(\ell) \\ &= \overline{\mathbf{z}}_{\text{mov}}(\ell) + \mathbf{n}\end{aligned} \tag{18}$$

and then performs adaptive Doppler estimation on the residual scattering.

Alternatively, following (18) with standard Doppler processing using some $\mathbf{W} = \mathbf{V}_{\overline{g}}$ as in (14) isolates the non-clutter responses for all G range intervals, with coherent gain occurring only for movers in the $\overline{g}^{\text{th}}$ designated range interval. This sequence of clutter cancellation and standard (non-adaptive) Doppler processing is equivalent to maximum SINR filtering [20].

B. Multi-Range RISR (MR-RISR)

The traditional formulation for the gain-constrained RISR filter bank [13] does not account for MTA in the RMMSE model constructed using (5), where the PRI is assumed long enough that MTA clutter can be ignored. That is, this naïve framework *ignores* the other $(G-1)$ range intervals. For the $\overline{g}^{\text{th}}$ range interval, the columns of the gain-constrained RISR filter bank are given by

$$\mathbf{w}_{\text{RISR},\overline{g},i}(f_{\text{nD}}) = \frac{\left(\mathbf{V}_{\overline{g}} \mathbf{P}_{\overline{g},i} \mathbf{V}_{\overline{g}}^H + \mathbf{R}_{\text{n}} \right)^{-1} \mathbf{v}_{\overline{g}}(f_{\text{nD}})}{\mathbf{v}_{\overline{g}}^H(f_{\text{nD}}) \left(\mathbf{V}_{\overline{g}} \mathbf{P}_{\overline{g},i} \mathbf{V}_{\overline{g}}^H + \mathbf{R}_{\text{n}} \right)^{-1} \mathbf{v}_{\overline{g}}(f_{\text{nD}})}, \tag{19}$$

where $\mathbf{P}_{\overline{g},i} = \left[\mathbf{x}_{\text{RISR},\overline{g},i} \mathbf{x}_{\text{RISR},\overline{g},i}^H \right] \odot \mathbf{I}_{M \times M}$ is the current power estimate of the Doppler response and $\mathbf{x}_{\text{RISR},\overline{g},i}$ denotes the RISR estimate at the i^{th} iteration.

Since (19) only accounts for a single range interval, scattering within other range intervals would degrade estimation. Modification of (19) to account for multiple range ambiguities based on the model of (6) should therefore provide enhanced MTA disambiguation. Consequently, if the $\mathbf{V}_g$ matrices are concatenated as

$$\mathbf{V} = [\mathbf{V}_1 \quad \mathbf{V}_2 \quad \cdots \quad \mathbf{V}_G], \tag{20}$$

then the first M entries for normalized Doppler f_{nD} of the gain-constrained multiple range (MR)-RISR filter become

$$\mathbf{w}_{\mathrm{MR-RISR},\bar{g},i}(f_{\mathrm{nD}}) = \frac{\left(\mathbf{V}\mathbf{P}_i\mathbf{V}^H + \mathbf{R}_{\mathrm{n}}\right)^{-1}\mathbf{v}_{\bar{g}}(f_{\mathrm{nD}})}{\mathbf{v}_{\bar{g}}^H(f_{\mathrm{nD}})\left(\mathbf{V}\mathbf{P}_i\mathbf{V}^H + \mathbf{R}_{\mathrm{n}}\right)^{-1}\mathbf{v}_{\bar{g}}(f_{\mathrm{nD}})}, \quad (21)$$

with $\mathbf{P}_i$ a block-diagonal combination of the individual $\mathbf{P}_{g,i}$ matrices. Collecting (21) for the N discretized Doppler shifts in $\mathbf{f}_{\mathrm{nD}}$ forms the filter bank $\mathbf{W}_{\mathrm{MR-RISR},\bar{g},i}$ for the $\bar{g}^{\mathrm{th}}$ range interval. Concatenating the filter banks for G range intervals ultimately forms the $M \times NG$ MR-RISR filter bank

$$\mathbf{W}_{\mathrm{MR-RISR},i} = \left[\mathbf{W}_{\mathrm{MR-RISR},1,i} \quad \mathbf{W}_{\mathrm{MR-RISR},2,i} \quad \cdots \quad \mathbf{W}_{\mathrm{MR-RISR},G,i}\right], \quad (22)$$

which yields simultaneous estimates of each range interval. MR-RISR can also be posed in the BaSC context via (18) as

$$\mathbf{x}_{\mathrm{MR-RISR},i}(\ell) = \mathbf{W}_{\mathrm{MR-RISR},i}^H\mathbf{z}(\ell) \quad (23)$$

to provide simultaneous clutter-cancelled estimates of each range interval.

IV. Experimental Results

Open-air measurements are used to experimentally assess effectiveness at distinguishing range-ambiguous movers via the Doppler processing techniques outlined in Section III. Here, we observe $G = 2$ range intervals using $T_{\mathrm{PRI}} = 4$ μs and $M = 10{,}000$ pulses (achieving $T_{\mathrm{CPI}} = 4$ ms) so that adequate energy-on-target is still achieved despite hardware constraints of low-power transmission. From a bridge on the University of Kansas campus, the intersections of 19th & Iowa St. (within the first range interval) and 21st & Iowa St. (within the second range interval) are illuminated at a center frequency of 3.45 GHz. Fig. 2 shows a map of the scene with points of interest labeled, where the regions between the adjacent red and green dots (0-150, 600-750 m) are blind ranges, regions bordering the blue dots (150-300, 450-600, 750-900, 1050-1200 m) are partially eclipsed, and regions between the blue dots (300-450, 900-1050 m) correspond to non-blind, non-eclipsed ranges. The red dots at 600 m and 1200 m represent the first and second range-ambiguous intervals (without the use of STC).

Three test cases were transmitted sequentially to capture the same movers for each case, allowing for comparison. The RF test setup was the Microwave Radar-in-a-Briefcase (MicRIB) system [26], which consists of an Nvidia Jetson Orin and an Ettus B200mini combined into a single portable arrangement. The system is low-cost, and consequently experiences not-insignificant degrees of phase noise and drift. These sources of model uncertainty effectively determine the limits of adaptive algorithm performance [9]. The MicRIB operates here with a 50 MHz transmit & receive sample rate, performing direct analog up-conversion of the baseband waveforms to the desired center frequency.

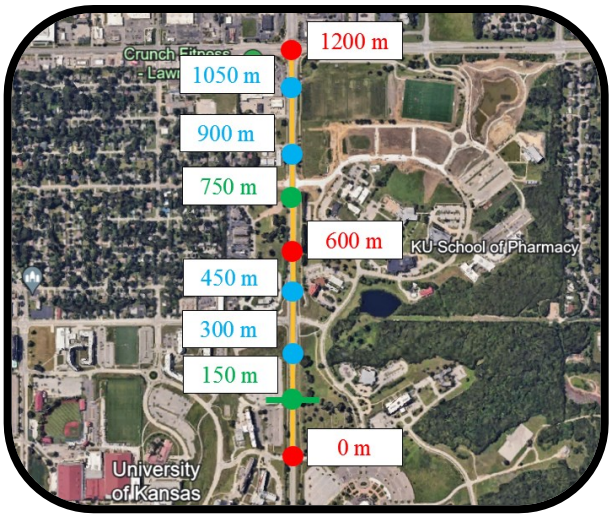

Fig. 2: Overhead view of the experimental demonstration scene for multiple range ambiguity separation with STC

Each of the three cases involve transmitting LFM waveforms with a 40 MHz swept bandwidth and 1 μs pulsewidth, yielding a time-bandwidth product of $TB = 40$. Case 1 does not incorporate STC, but instead uses a much longer PRI ($T_{\mathrm{PRI}} = 12$ μs) with the same number of pulses to establish "ground truth" scattering from both range intervals. Case 2 likewise does not incorporate STC and uses the shorter PRI ($T_{\mathrm{PRI}} = 4$ μs), thus experiencing folding of range ambiguities. Case 3 applies a uniformly random STC sequence to the shorter PRI, thereby providing a discriminant for range ambiguity separation.

Fig. 3 demonstrates the ground truth results from Case 1 when standard Doppler processing is applied. Movers are clearly visible at (93 m, –18.7 m/s), (225 m, –22.8 m/s), (210 m, 17.3 m/s), (216 m, 18 m/s), (387 m, 8.5 m/s), and (597 m, –17 m/s) in the first range interval and at (696 m, –20 m/s), (734 m, –19 m/s), and (905 m, –20 m/s) in the second range interval.

Fig. 4 then shows the standard Doppler processing response for Case 2. The movers in the partially eclipsed regions appear to be somewhat smeared. In fact, the mover at (597 m, –17 m/s) is no longer visible at all due to it aligning with a blind range (total eclipsing). Moreover, there is a noticeable 3× reduced Doppler resolution since the CPI is 3× shorter than in Case 1. This result serves as the "worst-case" for comparison purposes, since range disambiguation is impossible.

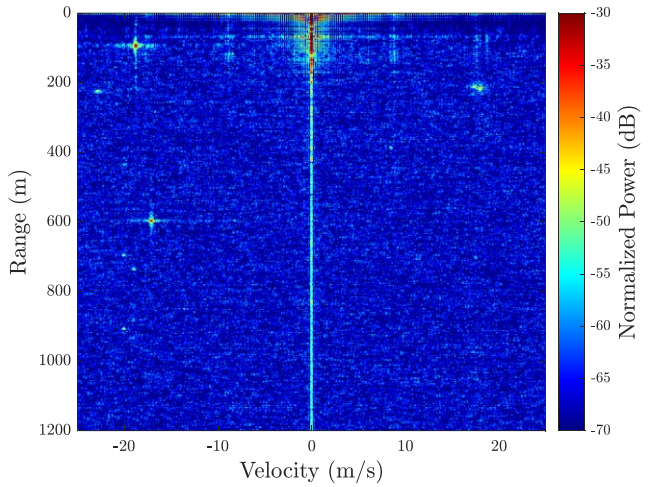

Fig. 3: Case 1 – No STC on the transmit waveform, $T_{\text{PRI}} = 12$ μs. Standard Doppler processing is applied, without clutter cancellation. Movers are visible in both range intervals.

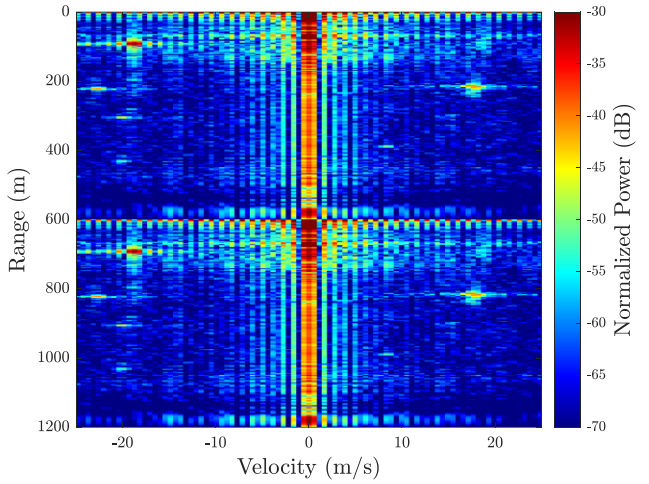

Fig. 4: Case 2 – No STC on the transmit waveform, $T_{\text{PRI}} = 4$ μs. Standard Doppler processing is applied, without clutter cancellation. Range disambiguation is not achieved.

In contrast, standard Doppler processing is applied to Case 3, as shown in Fig. 5. Suppression of range-folded scattering is on the order of $-10\log_{10}(M) = -40$ dB, though there is still residual power at ~600 m that is a consequence of the direct path leakage in range interval $g = 1$ partially correlating with the Doppler manifold in range interval $g = 2$. For the response shown in Figure 4, the mean relative power of the 600 m range cut is −40 dB.

Due to the stationarity of the scene, the superposition of the clutter responses is based on a simplified representation of expected internal clutter motion (modeled as Gaussian), from which the clutter covariance matrix of (16) can be obtained. When performing clutter cancellation prior to standard Doppler processing in Case 3, the response in Fig. 6 shows significant improvement. The zero-Doppler clutter components are cancelled, and the mean relative power at the 600 m range cut becomes −60 dB.

Now consider the application of the MR-RISR algorithm with 5 iterations to Case 3, as illustrated in Fig. 7. The range-folded direct path at 600 m is largely suppressed, with a mean relative power of −62 dB. Relative to the standard Doppler processing result (in Fig. 5), there is now significant sidelobe suppression for movers in the scene. The additional benefit introduced by clutter cancellation (combined with MR-RISR) is shown in Fig. 8. The mean relative power at the 600 m cut remains approximately the same, with a value of −62 dB.

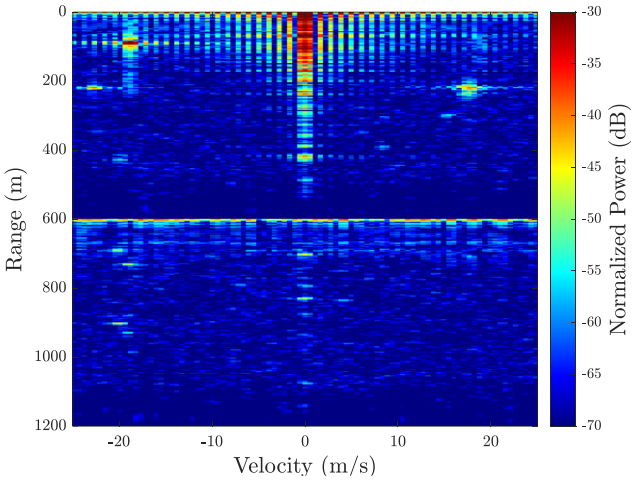

Fig. 5: Case 3 – Uniform random STC on the transmit waveform, $T_{\text{PRI}} = 4$ μs. Standard Doppler processing is applied, without clutter cancellation. Movers are visible in both range intervals, but now range-folded direct-path leakage is present at 600 m.

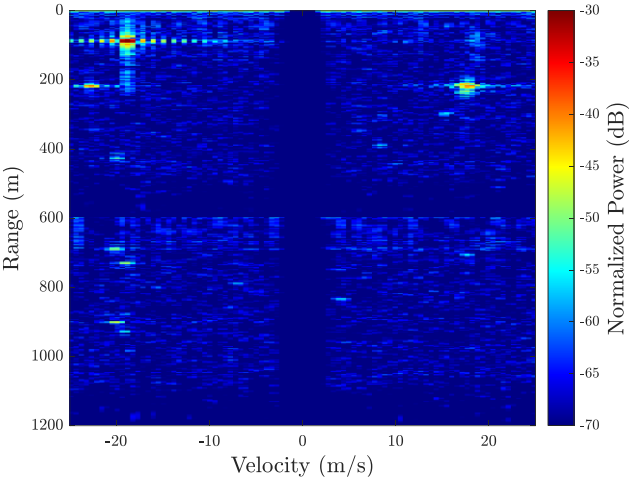

Fig. 6: Case 3 – Uniform random STC on the transmit waveform, $T_{\text{PRI}} = 4$ μs. Clutter cancellation is applied, followed by standard Doppler processing. Movers are visible in both range intervals, and the range-folded direct path at 600 m is greatly suppressed.

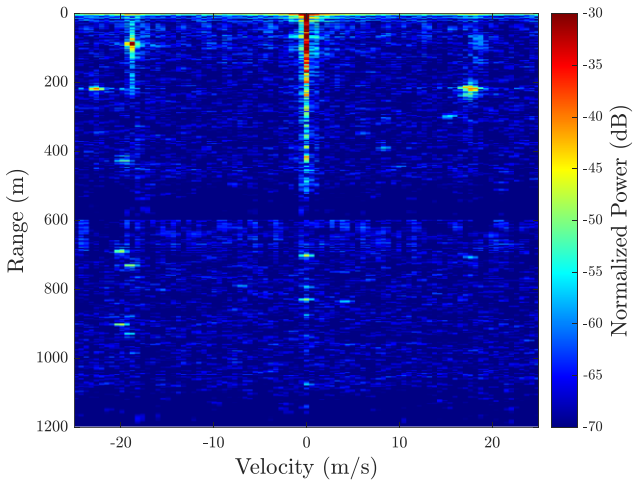

Fig. 7: Case 3 – Uniform random STC on the transmit waveform, $T_{\text{PRI}} = 4$ μs. MR-RISR is applied with 5 iterations, without clutter cancellation. Movers are visible in both range intervals, and Doppler sidelobes are suppressed. A slight degree of Doppler super-resolution is achieved.

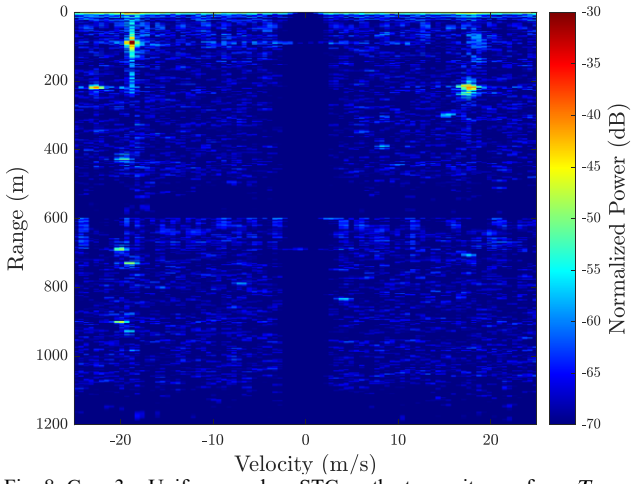

Fig. 8: Case 3 – Uniform random STC on the transmit waveform, $T_{\text{PRI}} = 4$ μs. Clutter cancellation is applied, followed by 5 iterations of MR-RISR. Movers are visible in both range intervals, and Doppler sidelobes are suppressed. A slight degree of Doppler super-resolution is achieved.

V. Conclusions

Through experimental demonstration, it has been shown that STC on transmit combined with RMMSE adaptive processing via RISR on receive pairs well to alleviate range ambiguities. The addition of clutter cancellation to adaptive estimation via the BaSC framework realizes a potentially useful way in which to isolate mover responses in a range-ambiguous setting.

References

[1] H. Sun, F. Brigui, M. Lesturgie, "Analysis and comparison of MIMO radar waveforms," *International Radar Conf.*, Lille, France, Oct. 2014.

[2] V. F. Mecca, D. Ramakrishnan, J. L. Krolik, "MIMO radar space-time adaptive processing for multipath clutter mitigation," *IEEE Workshop on Sensor Array and Multichannel Processing,* Waltham, MA, July 2006.

[3] W. van Rossum, L. Anitori, "Doppler ambiguity resolution using random slow-time code division multiple access MIMO radar with sparse signal processing," *IEEE Radar Conf.*, Oklahoma City, OK, Apr. 2018.

[4] N. Madsen, S. Cao, "Slow-time waveform design for MIMO GMTI radar using CAZAC sequences," *IEEE Radar Conf.*, Oklahoma City, OK, Apr. 2018.

[5] L. Anitori, J. Ender, "Waveform design for sparse signal processing in radar," *IEEE Radar Conf.*, Atlanta, GA, May 2021.

[6] J. Dall, A. Kusk, "Azimuth phase coding for range ambiguity suppression in SAR," *IEEE Intl. Geoscience & Remote Sensing Symposium,* Anchorage, AK, Sept. 2004.

[7] D.J. Rabideau, "Doppler-offset waveforms for MIMO radar," *IEEE Radar Conf.,* Kansas City, MO, May 2011.

[8] D.J. Rabideau, "MIMO radar waveforms and cancellation ratio," *IEEE Trans. Aerospace & Electronic Systems*, vol. 48, no. 2, pp. 1167-1178, Apr. 2012.

[9] S.D. Blunt, L.A. Harnett, B. Ravenscroft, R.J. Chang, C.T. Allen, P.M. McCormick, "Implications of diversified Doppler for random PRI radar," *IEEE Trans. Aerospace & Electronic Systems*, vol. 59, no. 4, pp. 3811-3834, Aug. 2023.

[10] H.L. Van Trees, *Optimum Array Processing: Part IV of Detection, Estimation, and Modulation Theory*, John Wiley & Sons, Inc., 2002.

[11] R.J. Chang, D.B. Herr, J.W. Owen, P.M. McCormick, S.D. Blunt, J.M. Stiles, "On the relationship between PRI staggering and sparse arrays," *IEEE Radar Conf.*, San Antonio, TX, May 2023.

[12] https://www.darpa.mil/program/beyond-linear-processing

[13] L.A. Harnett, B. Ravenscroft, S.D. Blunt, C.T. Allen, "Experimental evaluation of adaptive Doppler estimation for PRI-staggered radar," *IEEE Radar Conf.*, New York City, NY, Mar. 2022.

[14] C.C. Jones et al., "Development & experimental assessment of robust direction finding and self-calibration," *IEEE Radar Conf.*, New York City, NY, Mar. 2022.

[15] C.C. Jones, Z.E. Gannon, S.D. Blunt, C.T. Allen, A.F. Martone, "An adaptive spectrogram estimator to enhance signal characterization," *IEEE Radar Conf.*, New York City, NY, Mar. 2022.

[16] S.D. Blunt, K. Gerlach, "Adaptive pulse compression via MMSE estimation," *IEEE Trans. Aerospace & Electronic Systems*, vol. 42, no. 2, pp. 572-584, April 2006.

[17] T. Higgins, S.D. Blunt, A.K. Shackelford, "Time-range adaptive processing for pulse agile radar," *Intl. Waveform Diversity & Design Conf.*, Niagara Falls, ON, Canada, Aug. 2010.

[18] J. Harrington et al., "Challenges and prospective solutions for non-uniform radar waveforms in a shared spectrum," *IEEE Radar Conf.*, Denver, CO, May 2024.

[19] C.C. Jones, L.A. Harnett, C.A. Mohr, S.D. Blunt, C.T. Allen, "Structure-based adaptive radar processing for joint clutter cancellation and moving target estimation," *IEEE Intl. Radar Conf.*, Washington, DC, Apr. 2020.

[20] J. Ward, "Space-time adaptive processing for airborne radar," Lincoln Laboratory, Massachusetts Institute of Technology, Cambridge, MA, USA, Tech. Rep. ESC-TR-94-109, 1994.

[21] M.P. Hartnett, J.T. Clancy, R.J. Denton, "Utilization of a nonrecurrent waveform to mitigate range-folded spread Doppler clutter: application to over-the-horizon radar," *Radio Science*, vol. 33, no. 4., pp. 1125-1133, July/Aug. 1998.

[22] J.T. Clancy, H.F. Bascom, M.P. Hartnett, "Mitigation of range folded clutter by a nonrecurrent waveform," *IEEE Radar Conf.* Waltham, MA, Apr. 1999.

[23] F.L. Lin, M. Steiner, "New techniques for radar coherent range ambiguity resolution," *IEEE Radar Conf.*, Atlanta, GA, May 2001.

[24] W.W. Lee, "Radar space-time processing for range-folded spread-Doppler clutter mitigation," PhD dissertation, Duke University, 2011.

[25] D.P. Scholnik, "Range-ambiguous clutter suppression with pulse-diverse waveforms," *IEEE Radar Conf.*, Kansas City, MO, May 2011.

[26] J. Fraka, T. Higgins, J. Owen, "Real-time waveform-diverse pulse-Doppler demo via microwave radar-in-a-briefcase (MicRIB)," *IEEE Radar Conf.*, Denver, CO, May 2024.